Phase transitions and entropies for synchronizing oscillators

Martin Bier,[1,2] Bartosz Lisowski,[1,3] and Ewa Gudowska-Nowak[1,4]
[1]*M. Smoluchowski Institute of Physics, Jagiellonian University, ul. Łojasiewicza 11, 30-348 Kraków, Poland*
[2]*Department of Physics, East Carolina University, Greenville, North Carolina 27858, USA*
[3]*Unit of Pharmacoepidemiology and Pharmacoeconomics, Faculty of Pharmacy, Jagiellonian University Medical College, ul. Medyczna 9, 30-688 Kraków, Poland*
[4]*Mark Kac Center for Complex Systems Research and Malopolska Center of Biotechnology, Jagiellonian University, Gronostajowa 7A, 30-387 Kraków, Poland*
(Received 6 October 2015; published 25 January 2016)

We study a generic model of coupled oscillators. In the model there is competition between phase synchronization and diffusive effects. For a model with a finite number of states we derive how a phase transition occurs when the coupling parameter is varied. The phase transition is characterized by a symmetry breaking and a discontinuity in the first derivative of the order parameter. We quantitatively account for how the synchronized pulse is a low-entropy structure that facilitates the production of more entropy by the system as a whole. For a model with many states we apply a continuum approximation and derive a potential Burgers' equation for a propagating pulse. No phase transition occurs in that case. However, positive entropy production by diffusive effects still exceeds negative entropy production by the shock formation.

DOI: 10.1103/PhysRevE.93.012143

I. INTRODUCTION

The biological world offers many instances of systems where identical oscillators synchronize their phases due to a coupling. Examples include large groups of flashing fireflies [1], pacemaker cells in the heart [2], ensembles of neurons [3], a large number of pedestrians on a bridge [4], and metabolic oscillations of yeast cells in a suspension [5]. In these kind of systems analytical treatment commonly becomes manageable only when the coupling is small and can be mathematically treated as a perturbation [5–7]. Going from incoherent behavior to synchronized oscillators often takes the form of a phase transition as the coupling parameter is increased in value [6].

In this article we study the cyclic, four-state system that is depicted in Fig. 1. We assume a large total population N in the system and $p_i(t) = n_i(t)/N$, where $n_i(t)$ represents the population in state i at time t. This means that $p_i(t)$ can be associated with the probability to be in state i at time t. As the transitions are irreversible, the system is far from equilibrium. For the rates $k_i = k_{i\to i+1}$ we take

$$k_i = k_0 \exp[\alpha(p_{i+1} - p_{i-1})], \tag{1}$$

where α is a non-negative parameter that couples the probabilities (i.e., populations) in the different states.

The competition between diffusion and synchronization in the system depicted in Fig. 1 can be understood as follows. For $\alpha = 0$ there is no coupling and the stochasticity in the exponentially distributed transition times will result in a relaxation to $p_1 = p_2 = p_3 = p_4 = 1/4$ whatever the initial conditions are. However, if $\alpha > 0$ and if we have $p_1 = p_2 = \frac{1}{4}(1+\varepsilon)$ and $p_3 = p_4 = \frac{1}{4}(1-\varepsilon)$ (see Fig. 2) and at the same time $k_4 > k_2$ (see Fig. 1), then the diffusive effects can be counteracted. In that case the speeded up rate out of state 4 and the slowed down rate into state 3 will make the pulse in states 1 and 2 keep its shape.

How the coupling strength in Eq. (1) provides the counteraction to the diffusion can be seen as follows. Assume a pulse (high probability) concentrated in one state. If there is a more populated state ahead of the pulse as compared to behind, i.e., $p_{i+1} > p_{i-1}$, then the exponent in Eq. (1) is positive and the forward-moving-rate of the pulse is speeded up. The pulse will then swallow the state ahead. If, on the other hand, a less populated state is ahead and a more populated state is behind, i.e., $p_{i+1} < p_{i-1}$, then the forward rate of the pulse is slowed down and the population behind can merge with the pulse. In both cases there is a pull towards the pulse and the pulse acts like an absorber. The mechanism is somewhat mindful of the well-known Burgers' shock [8]. Ultimately, in a steady state, diffusion and accumulation balance each other out and the pulse travels around the cycle like a soliton in a time of approximately $4/k_0$.

A three-state version of the setup in Fig. 1 was numerically and analytically studied in Refs. [9–13]. In these works a mean-field approximation was applied and a Hopf bifurcation to synchronized behavior was found. It was furthermore analyzed how the system responds to disorder introduced on the level of the transition rates, demonstrating the rise of synchrony in a population of nonidentical units.

Four-state cycles occur frequently in biological systems. They are seen, for instance, in the ligand-gated and voltage-gated ion channels that maintain homeostasis and facilitate signal transduction [14]. A four-state system similar to the one in Fig. 1 was derived and studied in Ref. [15].

Interestingly, it has been described how different states of an ion channel involve different shapes that imply different stress and strain on the surrounding membrane [16]. Channels that operate in close proximity to each other could thus chemo-mechanically couple their kinetics. Our coupling parameter, α, could then reflect the strength of this interaction. We will come back to this idea in Sec. VI.

The setup of Fig. 1 gives rise to a three-dimensional system of coupled ODEs. A linear analysis [7] around the fixed point $p_1 = p_2 = p_3 = p_4 = 1/4$ leads to eigenvalues

$$\lambda_1 = -2k_0 \quad \text{and} \quad \lambda_{2,3} = \tfrac{1}{2}k_0\{(\alpha - 2) \pm i(\alpha + 2)\}. \tag{2}$$

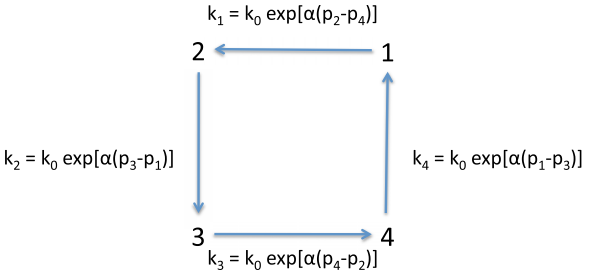

FIG. 1. The four-state system that is the subject of this article. The $j \to j+1$ transition rate depends on the populations in the states $j-1$ and $j+1$. We find a phase transition to a synchronized state as the coupling strength α is increased.

So, in the λ_1 direction, the fixed point $p_1 = p_2 = p_3 = p_4 = 1/4$ is an attractor. In the plane perpendicular to this axis, the real part of the complex eigenvalue changes sign, from negative to positive, at $\alpha = 2$, i.e., there is a supercritical Hopf bifurcation at $\alpha = 2$.

It is possible to rigorously derive how the amplitude ε depends on α with an expansion of the aforementioned 3D system of coupled ODEs. But here we give a simple and intuitive derivation to come to the same end result. Further on, we will use the idea behind our simple derivation as a guide to draw conclusions about entropy flow in the system.

Consider the scheme drawn in Fig. 2. For the pulse to stay compact and to not change shape, we need the flow $J_{4\to1}$ into the pulse to be equal to the flow $J_{2\to3}$ out of the pulse, i.e., $J_{4\to1} \approx J_{2\to3}$. Writing this as $p_2k_2 \approx p_4k_4$, substituting $p_2 = (1+\varepsilon)/4$, $p_4 = (1-\varepsilon)/4$, and taking the expressions for the rates k_2 and k_4 given in Eq. (1), we obtain:

$$\tfrac{1}{4}(1+\varepsilon)k_0 \exp[\alpha(p_3 - p_1)] \approx \tfrac{1}{4}(1-\varepsilon)k_0 \exp[\alpha(p_1 - p_3)], \tag{3}$$

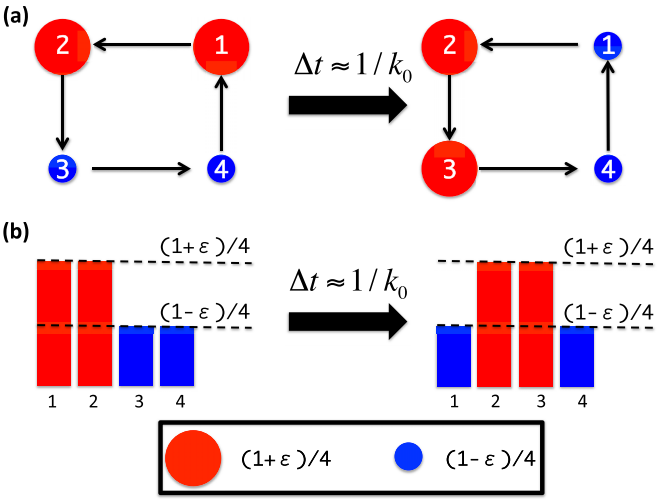

FIG. 2. For a sufficiently large value of the parameter α synchronization occurs in the setup of Fig. 1. (a) The ensuing pulse maintains its shape as it travels around the loop. (b) In the bottom graph the height of the bar indicates the probability to be in the corresponding state.

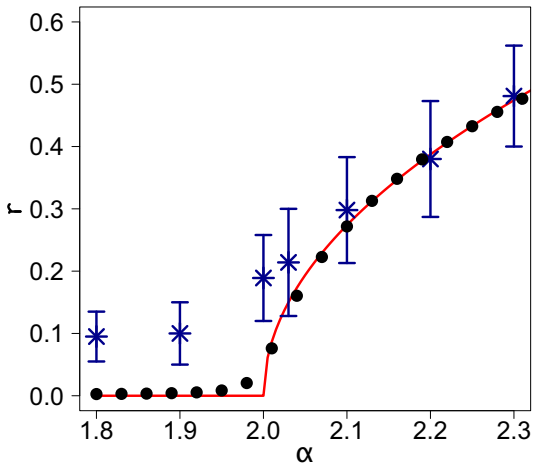

FIG. 3. The order parameter r as a function of the coupling strength α. The solid line shows the theoretical prediction [cf. Eq. (10)]. The black dots derive from the numerical solution of the system of ODEs that is associated with the kinetics of the system depicted in Fig. 1. We used $k_0 = 1$ and a time step of $\Delta t = 0.001$. The stars represent the results of stochastic simulations with $N = 1000$ units. For each value of α the stochastic simulation ran for $t = 150$ units of time. Error bars indicate the standard deviation.

which leads to

$$\frac{(1+\varepsilon)}{(1-\varepsilon)} \approx e^{\alpha\varepsilon}. \tag{4}$$

Solving for α, we find $\alpha \approx (1/\varepsilon)\ln[(1+\varepsilon)/(1-\varepsilon)]$. Next, expanding this expression in ε, we get $\alpha \approx 2 + \frac{2}{3}\varepsilon^2 + O(\varepsilon^4)$. Neglecting the higher-order contributions, we express the pulse amplitude ε in terms of the coupling strength α as:

$$\varepsilon \approx \sqrt{\frac{3}{2}(\alpha - 2)}. \tag{5}$$

In other words, there is a phase transition to a synchronized state at $\alpha = 2$. In Fig. 3 the order parameter, which will turn out to be linearly related to the amplitude ε, is depicted as a function of α. Equation (5) appears to be in good agreement with the results of simulations. The square-root or pitchfork shape at the bifurcation is found in a simple system such as $\dot{x} = x(\mu - x^2)$, but it also appears more generally in more complicated dynamical systems [17,18].

In Sec. II we study the order parameter that is associated with the transition to the synchronized state. In Sec. III we account for the entropy and the entropy production of the system.

Going back to the setup depicted in Fig. 1, we can identify the sequence . . . 1234123412 . . . with a continuous coordinate x. We let one unit of x correspond to the distance between two neighboring states.

Suppose that the counterclockwise transition rates in the system in Fig. 1 were all equal to a constant k_0. The transition time from one state into the next state then follows an exponential distribution with an average time and a standard deviation both equal to $1/k_0$. To take n steps around the four-step cycle takes an average time of $n(1/k_0)$. For subsequent steps, the variances $(1/k_0^2)$ add up. So with n steps we have

a standard deviation of $\sqrt{n}(1/k_0)$. In other words, if in time T the system takes an average of n steps, then there is an accompanying standard deviation of $\sqrt{n}$ steps.

In a time T ($\gg 1/k_0$) the pulse thus travels an average of about $k_0 T$ units of distance with a standard deviation of $\sigma = \sqrt{k_0 T}$ units of distance. For sufficiently many steps we have, by the central limit theorem, a spreading Gaussian for the probability density that travels in the positive direction:

$$\phi(x,t) = \frac{1}{\sqrt{2\pi k_0 t}} \exp\left[-\frac{(x-k_0 t)^2}{2k_0 t}\right]. \tag{6}$$

With a constant drift velocity k_0 and a linearly increasing variance $\sigma^2 = k_0 t = 2Dt$, we can consider this spreading Gaussian to be the solution of the following diffusion equation with diffusion coefficient $D = k_0/2$.

$$\phi_t = -k_0 \phi_x + D\phi_{xx}, \tag{7}$$

where $\phi = \phi(x,t)$ and the subscripts denote partial differentiation, i.e., $\phi_t = \partial_t \phi$, $\phi_x = \partial_x \phi$, and $\phi_{xx} = \partial_x^2 \phi$. Dedimensionalizing the time, Eq. (7) can be brought to the simple form $\phi_t = -\phi_x + \frac{1}{2}\phi_{xx}$.

The speeded up transition behind the pulse and the slowed down transition right ahead of the pulse is what counteracts the diffusive spread. In Sec. IV, we will show how the synchronization adds a nonlinearity to Eq. (7) and how the equation then effectively reduces to a Burgers' equation. In Sec. V we will derive the order parameter and entropy production associated with this partial differential equation (PDE). In Sec. VI we discuss our findings.

II. ORDER PARAMETER AS A FUNCTION OF COUPLING STRENGTH

In, for instance, the study of the Kuramoto model, the degree of synchronization is commonly described with the help of an order parameter [19]. In our case the order parameter takes the following form:

$$re^{i\psi} = \sum_{n=0}^{3} p_i e^{\frac{i\pi n}{2}}. \tag{8}$$

Obviously, r grows from 0 to 1 as the degree of synchronization increases. For the situation in the top panel of Fig. 2, it is easily inferred that

$$re^{i\psi} = \left(\frac{\varepsilon}{2}\sqrt{2}\right) e^{i\pi/4}. \tag{9}$$

As the pulse moves around the loop depicted in Fig. 1, $re^{i\psi}$ moves around the complex plane with the same time period.

With Eqs. (5) and (9) we derive for the order parameter as a function of α

$$r = \begin{cases} 0 & \text{if } \alpha < 2 \\ \frac{1}{2}\sqrt{3}\sqrt{\alpha - 2} & \text{if } \alpha > 2. \end{cases} \tag{10}$$

Figure 3 shows two simulation results and the theoretical prediction of Eq. (10). For one simulation we numerically solved the ODEs that describe the kinetics of the setup shown in Fig. 1. For the second simulation we performed stochastic simulations using a total of $N = 1000$ coupled units in the entire system and following a Gillespie algorithm [20,21]. In a Gillespie algorithm two random numbers are drawn at each time step. These numbers are used to select (i) the unit that changes its state according to the scheme from Fig. 1 and (ii) the time this transition would take. New values of transition rates [cf. Eq. (1)] and order parameter r are calculated after each time step. The simulations affirm the presence of a phase transition at $\alpha = 2$.

If the total population in the system in Fig. 1 is a finite number N, then we will not find $r = 0$ at $\alpha < 2$. This is due to the stochasticity in the transitions. We will next estimate what the bottom line value for r is, i.e., the value that we expect for $0 < \alpha < 2$. Taking a total population of 1, we see that a measurement will, on average, give the value $p = 0.25$ for each state. In that case the associated variance and standard deviation are $\sigma_1^2 = p(1-p) = 3/16$ and $\sigma_1 = \sqrt{3}/4$, respectively. With a total population of N, we have $N/4$ for the average population in each state. For the result of many subsequent and independent draws, the variances add up. So we have $\sigma_N^2 = Np(1-p) = 3N/16$ and $\sigma_N = \sqrt{3N}/4$. For the order parameter we thus expect an outcome:

$$re^{i\psi} = \sum_{n=0}^{3} \frac{1}{4}\left(\pm\frac{\sqrt{3}}{4\sqrt{N}}\right) e^{i\pi n/2}. \tag{11}$$

The $n = 0$ and $n = 2$ contribution to the sum are multiplied with, respectively, $e^0 = 1$ and $e^{i\pi} = -1$. Adding up the averages and the variances of these contributions, we obtain zero for the average real part and $\tilde{\sigma}_N^2 = 3/(8N)$ for the associated variance. This leads to $\tilde{\sigma}_N = \sqrt{3/(2N)}/2$ for the standard deviation. The $n = 1$ and $n = 3$ contributions in Eq. (11) give the same result for the imaginary part. The average value of both real and imaginary part is zero. But the average norm of both real part and imaginary part is not. With a zero-average Gaussian distribution, the average norm is:

$$\rho_{\mathrm{Re}} = \rho_{\mathrm{Im}} = \int_0^\infty \frac{2x}{\sqrt{2\pi}\tilde{\sigma}_N} \exp\left[-x^2/\left(2\tilde{\sigma}_N^2\right)\right] dx = \frac{2\tilde{\sigma}_N}{\sqrt{2\pi}}. \tag{12}$$

For the average value of r we thus come to the result

$$\langle r \rangle \approx \sqrt{\rho_{\mathrm{Re}}^2 + \rho_{\mathrm{Im}}^2} = \sqrt{\frac{3}{2\pi N}}. \tag{13}$$

We performed a Gillespie simulation with $N = 10000$ and $\alpha = 0$. It led to $r = 0.0090\,(\pm 0.0047)$. This is in good agreement with the $r = 0.0069$ that Eq. (13) predicts. Also for $N = 100$ and $N = 1000$ we obtained values for r at $\alpha = 0$ that confirm Eq. (13). The values observed in Fig. 3 for $\alpha < 2$ are well above the $r = 0.022$ that Eq. (13) predicts for $N = 1000$. This is because stochastic fluctuations die out ever more slowly as α is brought from 0 to 2. Simulations closer to the $N \to \infty$ and $t \to \infty$ limits should give results closer to the theoretical value of Eq. (13). The Gillespie simulations, however, require a lot of computation time.

III. ENTROPY PRODUCTION OF THE MOVING SYNCHRONIZED PULSE

Following Shannon [22], we take as the entropy per unit in the setup of Fig. 1 and Eq. (1):

$$S = -\sum_{i=1}^{4} p_i \ln p_i. \tag{14}$$

It is obvious that the situation with the pulse, as shown in Fig. 2, has a lower entropy than the $p_1 = p_2 = p_3 = p_4 = 1/4$ situation for which the entropy is maximal. When going from the situation on the left-hand side of Fig. 2 to the situation on the right-hand side of Fig. 2, there is no entropy change according to Eq. (14). However, the pulse has moved forward and what we have effectively done is performing a chemical cycle to move the pulse forward by one unit. We have converted chemical energy into mechanical work and there should be an associated entropy production. In this section we will account for the different entropy contributions.

Realizing that $\sum \dot{p}_i = 0$ as $\sum p_i = 1$ at all times, we infer from Eq. (14):

$$\dot{S} = -\sum_{i=1}^{4} \dot{p}_i \ln p_i. \tag{15}$$

This sum will not generally turn out equal to zero. This is because the term $\ln p_i$ adds weights to the flows $\dot{p}_i$ and, ultimately, the flows for small p_i are weighted more heavily.

We take the situation on the left side of Fig. 2, i.e., $p_1 = p_2 = (1+\varepsilon)/4$ and $p_3 = p_4 = (1-\varepsilon)/4$. We next take $\dot{p}_i = J_{i-1\to i} - J_{i\to i+1} = k_{i-1}p_{i-1} - k_i p_i$ and substitute into Eq. (15) the values for the rates k_i [cf. Eq. (1)]. We also substitute the $\alpha \approx (1/\varepsilon)\ln[(1+\varepsilon)/(1-\varepsilon)]$ that we found in the Introduction after Eq. (4). Summing over the four states and after some algebra it is then readily derived that $\dot{S}_{\text{synchr}} = 0$. This result is expected as the mechanism leading to Eq. (4) was formulated to lead to a pulse that stays intact.

In the derivation in the previous paragraph leading to $\dot{S}_{\text{synchr}} = 0$, we did not yet take the stochasticity into account. Each individual transition is a stochastic event and the result of a draw from an exponential distribution. Even with the irreversible transitions in Fig. 1, there is diffusion. The stochasticity in the transitions is giving us the spread of the distribution described in the Introduction and it produces temperaturelike behavior.

In the Introduction we saw that our system has an effective diffusion coefficient of $D = k_0/2$. Taking Fick's diffusion law ($\partial_t P = D\partial_x^2 P$) and writing it in the discrete form that is appropriate for the system in Fig. 1, we have

$$\dot{p}_i = \frac{k_0}{2}(p_{i+1} - 2p_i + p_{i-1}). \tag{16}$$

When this equation is applied to the situation depicted in Fig. 2, it is found that $\dot{p}_1 = \dot{p}_2 = -\varepsilon k_0/4$ and $\dot{p}_3 = \dot{p}_4 = \varepsilon k_0/4$. With again $p_1 = p_2 = (1+\varepsilon)/4$ and $p_3 = p_4 = (1-\varepsilon)/4$ and applying Eq. (15), the entropy production by the diffusion, at the lowest order in ε, is found to be

$$\dot{S}_{\text{diff}} = k_0\varepsilon^2 = \tfrac{3}{2}k_0(\alpha - 2) = 2k_0 r^2. \tag{17}$$

We thus see that, for $\alpha > 2$, the moving pulse is associated with a net production of entropy. The entropy production increases with the pulse amplitude ε and the associated order parameter r. It needs to be emphasized here again that the entropy production of the moving pulse is not associated with a deterioration of the moving pulse. The pulse stays intact. But as was already explained in the Introduction, it is the fluctuations in the speed of the pulse that make the process nondeterministic and expand the available phase space. Of course, with $p_1 = p_2 = p_3 = p_4 = 1/4$ there is no pulse and no such phase space expansion occurs.

For $0 < \alpha < 2$ we have $p_1 = p_2 = p_3 = p_4 = 1/4$ and an associated entropy of $S = 2\ln 2$ [cf. Eq. (14)]. With the distribution shown in Fig. 2, the entropy is obviously smaller. Taking $\ln(1 \pm \varepsilon) \approx \pm\varepsilon - \varepsilon^2/2$ for the lowest orders in ε, we find that for $\alpha > 2$ and small ε

$$S \approx 2\ln 2 - \varepsilon^2/2. \tag{18}$$

In other words, the formation of the pulse represents a symmetry breaking and a self-organized establishment of order. However, as we will show in the next paragraphs, the pulse allows the system as a whole to produce more entropy.

The transitions in Fig. 1 dissipate energy and produce entropy. This is obvious for the case of chemical transitions; the more irreversible such a transition, i.e., the larger the ratio of the forward and backward transition rate, the more entropy the forward transition produces.

If $p_1 = p_2 = p_3 = p_4 = 1/4$, each transition rate in Fig. 1 equals k_0 and the average turnover of the system equals $\Sigma_{i=1}^4 p_i k_0 = k_0$. For the situation sketched in Fig. 2 there are two transition rates that take on the value $k_0 \exp[\alpha\varepsilon/2]$ and two transition rates that take on the value $k_0 \exp[-\alpha\varepsilon/2]$. This leads to an average transition rate of $\langle k\rangle = k_0 \cosh[\alpha\varepsilon/2]$. The functions $f(x) = e^x$ and $f(x) = e^{-x}$ have positive second derivatives, i.e., they are concave up. It is essentially because of Jensen's theorem ($\langle f(x)\rangle > f(\langle x\rangle)$ if $f''(x) > 0$, see Ref. [23]) that we have $\langle k\rangle > k_0$. More importantly, also the average turnover for the entire system, i.e., $\Sigma_{i=1}^4 p_i k_i$, evaluates to $k_0 \cosh[\alpha\varepsilon/2]$ with the synchronized pulse as in Fig. 2.

We observe that not having a flat (maximal entropy) distribution helps the open system to ultimately achieve a higher turnover. The lower-entropy synchronized pulse is essentially an investment; eventually it acts like a catalyst for an enhanced turnover and increased entropy production rate. In this sense the pulse is a self-organized dissipative structure as described by Prigogine [24].

IV. SYNCHRONIZED PULSE AS A BURGERS' SHOCK

When increasing the number of states in a cycle as in Fig. 1, we encounter ever larger systems of equations. Instead of taking this route with all its analytical and numerical complications, it may be more fruitful to examine the other end. We thus take a cycle with a large number of states n and go to the continuum limit that we already briefly discussed in the Introduction.

In the cycle depicted in Fig. 4 there are n states. In the vicinity of the phase transition we have $\phi(j,t) = O(1/n)$, for the probability in each state j. For a smooth, small-amplitude pulse (in the next section we explore a sinusoidal modulation)

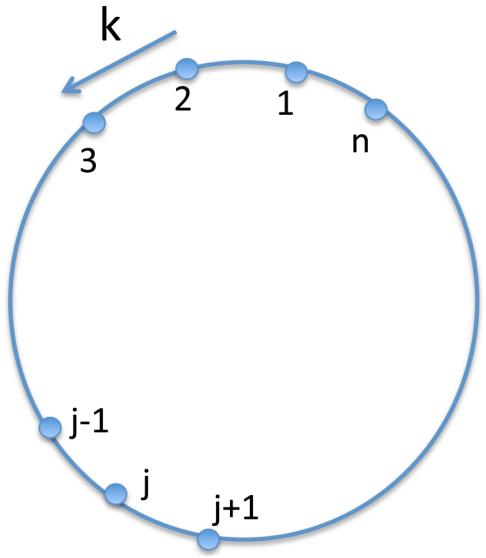

FIG. 4. An n-state generalization of the system shown in Fig. 1.

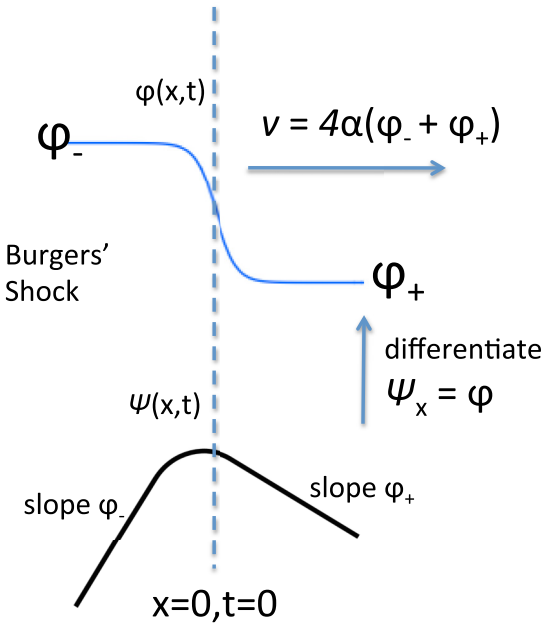

FIG. 5. The top graph shows the propagating Burgers' shock [Eq. (24)]. The speed of the shock front depends on the shock amplitude and on the parameter α. The bottom graph shows the antiderivative with respect to x of the Burgers' shock [Eq. (25)], which represents the soliton solution of the equations associated with the system depicted in Fig. 4. A robust synchronized pulse travels around the cyclic setup.

we have $(\phi_{\max} - \phi_{\min}) = O(1/n)$ for the maximal and minimal ϕ. For the horizontal distance between the maximum and the minimum, we, moreover, have $|x_{\max} - x_{\min}| = O(n)$. This leads to $\phi_x = O(1/n^2)$ and $\phi_{xx} = O(1/n^3)$.

Next we enter the ϕ dependence of k as given in Eq. (1). For the continuous equivalent of Eq. (1) it is found that

$$k = k_0 \exp\{\alpha[\phi(x+1,t) - \phi(x-1,t)]\}. \tag{19}$$

For a slowly varying $\phi(x,t)$ a simple, 1st order approximation is justified and gives $\phi(x+1,t) - \phi(x-1,t) = 2\phi_x(x,t)$. After $\exp\{\alpha[\phi(x+1,t) - \phi(x-1,t)]\} \approx 1 + 2\alpha\phi_x(x,t)$, we are thus led to the following nonlinear PDE:

$$\phi_t = -k_0\phi_x - 2k_0\alpha\phi_x^2 + \tfrac{1}{2}k_0\phi_{xx} + k_0\alpha\phi_x\phi_{xx}. \tag{20}$$

We first notice that $\phi_x\phi_{xx} = O(1/n^5)$. The $\phi_x\phi_{xx}$ term is smaller than the other terms on the right-hand side and we therefore neglect it. With a Galilean transformation the $k_0\phi_x$ term can be removed. To go to $\psi(x',t) = \phi(x,t)$, where $x' = x - k_0 t$, we formally take

$$x' = \mu(x,t) = x - k_0 t \quad t' = \nu(x,t) = t. \tag{21}$$

With the standard Jacobian matrix approach we then have:

$$\begin{pmatrix}\phi_x \\ \phi_t\end{pmatrix} = \begin{pmatrix}\mu_x & \nu_x \\ \mu_t & \nu_t\end{pmatrix}\begin{pmatrix}\psi_{x'} \\ \psi_{t'}\end{pmatrix},$$

where $\mu_x = \partial x'/\partial x = 1$, $\nu_x = \partial t'/\partial x = 0$, $\mu_t = \partial x'/\partial t = -k_0$, and $\nu_t = \partial t'/\partial t = 1$. From here it is inferred that $\phi_x = \psi_{x'}$ and $\phi_t = \psi_{t'} - k_0\psi_{x'}$. Substituting this, dropping the primes, and absorbing $2k_0$ into the timescale, we obtain for the new equation in the new inertial frame

$$\psi_t = -4\alpha\psi_x^2 + \psi_{xx}. \tag{22}$$

This is actually a well-known equation. It is generally known as the potential Burgers' equation [25]. By taking the partial derivative with respect to x on both sides and next taking $\psi_x = \varphi$, the original Burgers' equation is retrieved for $\varphi = \varphi(x,t)$:

$$\varphi_t = -8\alpha\varphi\varphi_x + \varphi_{xx}. \tag{23}$$

The potential Burgers' equation, Eq. (22), is actually linearizable. The linear diffusion equation $\eta_t = \eta_{xx}$ turns into the above Eq. (22) after taking $\eta(x,t) = \exp[-4\alpha\psi(x,t)]$.

Equation (23) supports soliton solutions (cf. Fig. 5):

$$\varphi(x,t) = \frac{\varphi_- + \varphi_+}{2} - \frac{\varphi_- - \varphi_+}{2}\tanh[2\alpha(\varphi_- - \varphi_+)(x - vt)], \tag{24}$$

where we have for the speed of the soliton, as indicated in Fig. 5, $v = 4\alpha(\varphi_- + \varphi_+)$. The quantity $[2\alpha(\varphi_- - \varphi_+)]^{-1}$ is known as the thickness of the shock. A good explanation of these dynamics is also found in Ref. [26].

Integrating the solution for $\varphi(x,t)$, we obtain $\psi(x,t)$:

$$\psi(x,t) = \left(\frac{\varphi_- + \varphi_+}{2}\right)x - \frac{1}{4\alpha}\ln\{\cosh[2\alpha(\varphi_- - \varphi_+) \times (x - vt)]\} + \psi(0,t), \tag{25}$$

where $\psi(0,t)$ is the constant of integration.

It is important to notice that the phase transition that was identified in the discrete system is not present in the above continuous version. There is no phase transition or bifurcation associated with the soliton depicted in Fig. 5 and described in Eqs. (22)–(25). For $\alpha = 0$, Eqs. (22) and (23) reduce to an ordinary diffusion equation. As α is increased from zero, what we see is the development of an ever steeper shock front in the top panel of Fig. 5 and an ever more pronounced synchronization hump in the bottom panel of Fig. 5. With an increasing α, also the speed of the pulse increases. Unlike for the case of the three-state and four-state system, the continuous

case offers no relation between the amplitude of the pulse, $(\varphi_- - \varphi_+)$, and the coupling parameter α.

V. ENTROPY PRODUCTION AND ORDER PARAMETER AS THE SOLITON PROPAGATES

For ordinary diffusion without drift, we have for a particle that starts at $x = 0$ at $t = 0$:

$$\Phi(x,t) = \frac{1}{\sqrt{4\pi Dt}} e^{-\frac{x^2}{4Dt}}. \tag{26}$$

For this case the entropy $S(t)$ is readily evaluated as

$$\begin{aligned} S(t) &= -\int_{-\infty}^{+\infty} \Phi(x,t) \ln \Phi(x,t)\, dx \\ &= \int_{-\infty}^{+\infty} \frac{e^{-\frac{x^2}{4Dt}}}{\sqrt{4\pi Dt}} \left(\frac{x^2}{4Dt} + \ln \sqrt{4\pi Dt} \right) dx \\ &= \frac{1}{2}[1 + \ln(4\pi Dt)], \end{aligned} \tag{27}$$

which leads to $\dot{S}(t) = 1/(2t)$ [27]. That the diffusion entropy follows $S \propto \frac{1}{2} \ln t$ can also be understood from more intuitive arguments. Boltzmann's definition of the entropy, $S = k \ln \Omega$, tells us that the entropy is proportional to the logarithm of the volume Ω of the available phase space. If we identify this available phase space volume with the standard deviation of the Gaussian, then $\Omega \approx \sqrt{\langle x^2 \rangle}$. As $\langle x^2 \rangle \propto t$ for normal diffusion, we have $S \propto \ln \sqrt{t} = \frac{1}{2} \ln t$.

It should be realized that Eqs. (14) and (15) come with a little caveat when we go to continuous x. For a periodic $\psi(x,t)$ (period L) the entropy is maximal when the probability distribution is flat, i.e., $\Phi_0 = 1/L$. Our definition of the entropy is the commonly used Kullback-Leibler distance, which effectively measures how far away we are from this flat distribution [28]:

$$S(t) = -\int_{x0}^{x0+L} \Phi(x,t) \ln \left(\frac{\Phi(x,t)}{\Phi_0} \right) dx. \tag{28}$$

By normalizing the period, i.e., $x \to x/L$ and $\Phi \to L\Phi$, we can work with entropy as simply $S = -\int \Phi \ln \Phi\, dx$, where the integration runs over the unity period.

Equation (22), the potential Burgers' equation, was arrived at after a linear Galilean transformation. It is easy to show that no entropy production is involved in a linear traveling wave. Take the PDE $\Phi_t = \Phi_x$. To obtain the rate of change for the entropy we perform

$$\frac{dS}{dt} = -\frac{d}{dt} \int \Phi \ln \Phi\, dx = -\int \dot{\Phi}(\ln \Phi + 1)\, dx, \tag{29}$$

where the integration runs over one period. For Φ periodic in x we obviously have $\int \dot{\Phi}\, dx = 0$ when the integration runs over one spatial period. For the other term in Eq. (29) we derive

$$\begin{aligned} \int \dot{\Phi} \ln \Phi\, dx &= \int \Phi_x \ln \Phi\, dx = \int \ln \Phi\, d\Phi \\ &= \Phi(\ln \Phi - 1)| = 0. \end{aligned} \tag{30}$$

So the Galilean transformation that removed ϕ_x from the right-hand side of Eq. (20) is without consequence for the entropy analysis.

Next we take Eq. (22) and write down for the entropy production

$$\begin{aligned} \frac{dS}{dt} &= -\frac{d}{dt} \int \psi \ln \psi\, dx \\ &= -\int \dot{\psi}(\ln \psi + 1)\, dx \\ &= \int \left(4\alpha \psi_x^2 - \psi_{xx}\right) \ln \psi\, dx. \end{aligned} \tag{31}$$

We will evaluate both terms.

The integrand $\psi_x^2 \ln \psi$ is associated with the shock formation. The integrand $\psi_{xx} \ln \psi$ is associated with the diffusion. The shock term is supposed to give a negative contribution to the entropy production as it accumulates probability density and drives the system away from the homogeneous spread. As we saw before, diffusion produces entropy. So $\psi_{xx} \ln \psi$ should be positive.

The integral $\int \psi_x^2 \ln \psi\, dx$ cannot be further simplified. So we have

$$\dot{S}_{\text{shock}} = 4\alpha \int \psi_x^2 \ln \psi\, dx. \tag{32}$$

The diffusion term can be simplified through integration by parts

$$\dot{S}_{\text{diff}} = -\int \psi_{xx} \ln \psi\, dx = \int \psi_x\, d(\ln \psi) = \int \psi_x^2 \left(\frac{1}{\psi} \right) dx. \tag{33}$$

As ψ_x^2 and $(1/\psi)$ are both positive, the integral (33) will indeed always be positive.

The most obvious approximation for the shape of the synchronized pulse in the continuous domain would be a harmonic one. We take a unit period and a small ε for the amplitude of the pulse in the vicinity of the phase transition. For the $t = 0$ situation we take

$$\psi(x,0) = 1 + \varepsilon \cos(2\pi x). \tag{34}$$

With Eq. (34) we have at the lowest order for the pertinent terms [cf. Eqs. (32) and (33)]:

$$\begin{aligned} \psi_x^2 &\approx 4\pi^2 \varepsilon^2 \sin^2(2\pi x), \\ \ln \psi &\approx \varepsilon \cos(2\pi x) - \frac{\varepsilon^2}{2} \cos^2(2\pi x), \\ \text{and } \frac{1}{\psi} &\approx 1 - \varepsilon \cos(2\pi x). \end{aligned} \tag{35}$$

With these approximations we are led to

$$\dot{S}_{\text{shock}} \approx -\alpha \pi^2 \varepsilon^4 \quad \text{and} \quad \dot{S}_{\text{diff}} \approx 2\pi^2 \varepsilon^2. \tag{36}$$

We thus observe that for the propagating pulse the negative entropy production occurs at a higher order in the small parameter ε than the entropy production. The propagation of a synchronized pulse, we conclude, is associated with a net production of entropy. This is what we would expect as the irreversible chemical transitions that drive the cycle in Fig. 4 dissipate energy and imply a production of entropy.

Recently Nordenfelt applied similar reasoning and techniques to evaluate the entropy production for a synchronizing system described by a PDE [29]. His system, however, is more

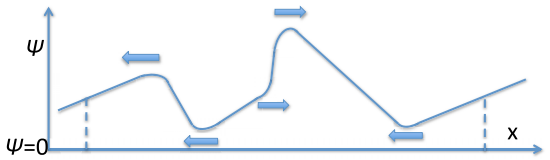

FIG. 6. The density $\psi(x,t)$ can exhibit multiple synchronizations. The cusps in $\psi(x,t)$ can be identified with solitons (this is obvious upon considering ψ_{xx} when the cusps become pulses). These solitons can have different velocities. The velocity of a soliton is proportional to the sum of the slopes to the left and right of the cusp (see Fig. 5). Directions thus obtained are indicated by arrows. The dashed vertical lines indicate one period, i.e., one cycle in Fig. 4.

complicated as it also involves a continuum of characteristic frequencies.

The order parameter in case of a harmonic approximation as in Eq. (34) is easily evaluated. We find it to be linear in ε:

$$r = \int_{-1/2}^{1/2} (1 + \varepsilon \cos[2\pi x]) e^{i2\pi x}\, dx = \frac{\varepsilon}{2}. \tag{37}$$

The continuous case that we studied in this and the previous section differs from the finite-state model in that there is no emerging simple relation between the amplitude of the pulse and the coupling parameter α. There is also no phase transition for the continuous case. In the case of $\alpha = 0$ there is no synchronization and the system in Fig. 4 moves in the counterclockwise direction making on average k_0 transitions per unit of time. After the Galilean transformation that we performed [cf. Eq. (21)], the frame moves around the circle with the same speed k_0. It is in that frame that we were led to Fig. 5 and Eqs. (22) and (23).

The variable $\psi(x,t)$ [cf. Eq. (22)] represents a probability density and therefore has to be positive everywhere. The variable $\psi(x,t)$ must, furthermore, give unity when integrated over the entire cycle in Fig. 4. But within these restrictions it is still possible, for $\alpha > 0$, that multiple synchronizations are present. Figure 5 and the solution Eq. (25) make clear how the cusps can be identified with moving solitons. Figure 6 shows how these solitons can propagate at different speeds and in either direction. In other words, the coupling can both speed up and slow down the turnover rate in Fig. 4. Because of the nonlinear character of Burgers' equation, no simple superposition of solutions applies. Different solitons interact when they collide. If the diffusive part of Burgers' equation is small relative to the nonlinear term, the solitons appear to collide inelastically and mimic the behavior of sticky gas particles [30].

Schemes with subsequent conformational changes as in Fig. 1 are, of course, simplifications. Going back to the ion channels that we mentioned in the Introduction, we have to realize that an ion channel is a big complicated protein and that what we take to be a discrete transition is, in actuality, continuous diffusive motion through a corridor in a many-dimensional conformational space. An 18-state model has been applied to describe the activity of the $\alpha 1\beta$ glycine receptor [31]. At that point discrete models have lost their computational simplicity and intuitiveness. It may well be that biological reality is ultimately better described with a continuous-type model as presented in Secs. IV and V.

VI. DISCUSSION

In this article we first studied how diffusion and accumulation compete in a four-state system as described in Fig. 1 and Eq. (1). Like in a three-state system [9–13], a sharp phase transition is observed as the coupling parameter α is varied. We next went to an n-state system and studied an $n \to \infty$ continuum limit.

There is an ongoing and intense research interest in the synchronization behavior of systems like the one in Fig. 1 [32,33]. We chose our rates k_i to depend on the populations p_i as in Eq. (1), because in chemical kinetics energies commonly are linearly related to logarithms of rates. But other dependencies are possible. Linear dependencies, $k_i \propto (1 + bp_{i+1})$, have been explored with a smaller population [34]. Combinations of rates and fixed waiting times have also been explored [35]. In Ref. [36] the replication that is found in biological systems is modeled through an increasing population.

In most works on coupled oscillators the focus is on the bifurcation structure of the system. Much of our focus here has been on the thermodynamics of the synchronizing oscillators and in particular on the production and the flow of entropy. Commonly the mathematics of synchronizing oscillators can get very convoluted. Through approximations we have attempted to keep the formulas concise and intuitive, while still describing the phenomena.

As the transitions in Fig. 1 are irreversible, there is a net production of entropy as the system is cycling. The net production of entropy should also emerge from the synchronization kinetics of the system depicted in Fig. 1. The formation of a phase-synchronized pulse actually involves an increase of the order parameter. However, we have shown that in the vicinity of the phase transition there is still a net positive production of entropy. We have furthermore shown that the phase synchrony can be thought of as a dissipative structure: accumulation of units actually leads to a higher rate for the entropy-producing transitions in Fig. 1.

When a cycle as in Fig. 1 consists of a continuum of states (cf. Fig. 4), the PDEs that are the focus of Secs. IV and V constitute the proper way of description. It is remarkable that the Burgers' equation that we derive as the appropriate continuization no longer exhibits the phase transition as the coupling parameter α is varied. No relation between the pulse amplitude ε and the system parameters is apparent from the theory.

It may be surprising that the phase transition is no longer present in the continuum limit. When, for instance, the similar and well-known Kuramoto model is taken to its continuum limit [19], a phase transition as in our Fig. 3 remains present. But there is a difference between the continuum Kuramoto model and our ultimate Burgers'-like model. From the governing equation of the Kuramoto model,

$$\dot{\theta}_i = \omega_i + \frac{K}{N} \sum_{j=1}^{N} (\theta_j - \theta_i), \tag{38}$$

it is obvious that every single one of the N units is coupled to every other unit on the circle. In our setup a unit in state i is coupled only to units in neighboring states $i-1$ and $i+1$. For the four-state system these two neighbor states still constitute half of the total number of states and interactions can then still be considered global in nature. But as the number of states increases to a large n (cf. Fig. 4), the neighbor-neighbor interactions take on an ever more local character. It is possible to get global phase transitions with just local interactions. Ising models provide a well-understood example of this. But this is not what happens in Burgers' equation [37].

In Sec. V we derived how the propagating soliton produces entropy. We see that for a small pulse amplitude ε, the production of negative entropy associated with the shock-formation term in the PDE is of a higher order in ε than the positive entropy production diffusion term.

Soliton propagation is not necessarily always associated with entropy production. Apply, for instance, the transformation $t \to -t$ to Burgers' equation (23). In that case the soliton depicted in Fig. 5 will simply move in the reverse direction and with the same speed. Such a soliton, however, would also be a solution to a PDE with antidiffusion (a minus sign in front of the second partial derivative with respect to x) and shock dissolution (negative α). For such a soliton the propagation involves the production of negative entropy.

The moving solitons that we derive are still entropy-producing structures. However, they may slow down the turnover rate (cf. Fig. 4) as compared to the setup that has no coupling (i.e., $\alpha = 0$). So these synchronization solitons are no longer the catalysts for enhanced turnover that they were in the finite-state case.

It is instructive to examine the relation of our analysis to the aforementioned conformational coupling of nearby ion channels in a membrane. Multistate models, such as the one introduced in Fig. 1, are commonly used to describe the kinetics of ion channels [15]. Collective action of such channels has been observed in numerous experiments [38–40], but the underlying mechanism by which the membrane proteins communicate is still not obvious.

It has been suggested that information about a channel's state is transmitted via the membrane between the channels. It is indeed not hard to imagine that the different states of a channel are geometrically different. If channels are sufficiently close and if the lipid-bilayer membrane and the cytoskeletal structures in which they are embedded are sufficiently stiff, then channels could, in principle, be coupled chemomechanically and kinetics as in Fig. 1 could ensue [16,41–44]. Of course, such conformational coupling through membrane deformation only works for short distances.

Another possible way to couple closely spaced channels is through the electrochemical gradient between the two sides of the membrane. An open ion channel results in a local change of the transmembrane potential. The more open channels in a small area, the bigger the resulting change in the electric field. As electrochemical potentials can affect opening and closing of a channel [45], feedback loops can be established. This is how action potentials arise and propagate [46]. It is also how kinetics like in Fig. 1 can emerge.

Clusters of ion channels, where the action of one channel is amplified by the actions of the neighboring ones, have been found in many cell types. It has even been observed how such clustering is regulated during cell development [47,48]. Proper clustering of different kinds of channels in Ranvier nodes of myelinated nerve fibers appears to be essential for achieving a good propagation of action potentials [49]. In experimental studies on synaptic transmission it has been shown that having receptor clusters of variable sizes optimizes the response to small stimuli and the sensitivity to signal amplitude [50]. In their analysis of a theoretical model of the action of inositol 1,4,5-triphosphate receptors in a plasma membrane, Shuai and Jung found that channel clustering can dramatically enhance a cell's capability of creating a large Ca^{2+} response to a weak stimulation [51].

The coupling parameter α that we introduced could be associated with the density of channels in a cluster and with the average distance of channels in a cluster. Experimental studies to establish an explicit quantitative relation between a coupling parameter and a signal amplitude should be feasible. Our results can be a guideline when performing such studies of the collective action of ion channels. It would be particularly interesting if something as dramatic as a phase transition could be experimentally established.

ACKNOWLEDGMENTS

E.G.N. and B.L. gratefully acknowledge the National Science Center, Poland for the grant support (2014/13/B/ST2/02014) that made this work possible.

[1] J. Buck and E. Buck, Sci. Am. **234**, 74 (1976).
[2] C. S. Peskin, *Mathematical Aspects of Heart Physiology* (Courant Institute of Mathematical Science Publication, New York, 1975).
[3] B. Lindner and L. Schimansky-Geier, Phys. Rev. Lett. **86**, 2934 (2001).
[4] B. Eckhardt, E. Ott, S. H. Strogatz, D. M. Abrams, and A. McRobie, Phys. Rev. E **75**, 021110 (2007).
[5] M. Bier, B. M. Bakker, and H. V. Westerhoff, Biophys. J. **78**, 1087 (2000).
[6] A. T. Winfree, J. Theoret. Biol. **16**, 15 (1967).
[7] J. D. Murray, *Mathematical Biology*, 2nd Corrected Ed. (Springer-Verlag, New York, 1993).
[8] E. Atlee Jackson, *Perspectives of Nonlinear Dynamics* (Cambridge University Press, New York, 1991), Vol. 2.
[9] K. Wood, C. Van den Broeck, R. Kawai, and K. Lindenberg, Phys. Rev. Lett. **96**, 145701 (2006).
[10] K. Wood, C. Van den Broeck, R. Kawai, and K. Lindenberg, Phys. Rev. E **74**, 031113 (2006).
[11] K. Wood, C. Van den Broeck, R. Kawai, and K. Lindenberg, Phys. Rev. E **75**, 041107 (2007).

[12] K. Wood, C. Van den Broeck, R. Kawai, and K. Lindenberg, Phys. Rev. E **76**, 041132 (2007).
[13] K. Wood, C. Van den Broeck, R. Kawai, and K. Lindenberg, in *Nonequilibrium Statistical Mechanics and Nonlinear Physics*, edited by O. Descalzi, O. A. Rosso, and A. Larrondo, AIP Conf. Proc. No. 913 (AIP, Melville, NY, 2007).
[14] D. Colquhoun, K. A. Dowsland, M. Beato, and J. R. Plested, Biophys. J. **86**, 3510 (2004).
[15] H. Flyvbjerg, E. Gudowska-Nowak, P. Christophersen, and P. Bennekou, Acta Phys. Pol. B **43**, 2117 (2012).
[16] T. Ursell, K. C. Huang, E. Peterson, and R. Phillips, PLoS Comput. Biol. **3**, e81 (2007).
[17] E. Atlee Jackson, *Perspectives of Nonlinear Dynamics* (Cambridge University Press, New York, 1991), Vol. 1.
[18] J. Guckenheimer and P. Holmes, *Nonlinear Oscillations, Dynamical Systems, and Bifurcations of Vector Fields* (Springer-Verlag, New York, 1983).
[19] S. H. Strogatz, Physica D **143**, 1 (2000).
[20] D. T. Gillespie, J. Comput. Phys. **22**, 403 (1976).
[21] D. T. Gillespie, J. Phys. Chem. **81**, 2340 (1977).
[22] C. E. Shannon and W. Weaver, *The Mathematical Theory of Communication* (University of Illinois Press, Champaign, 1998).
[23] H. L. Royden and P. M. Fitzpatrick, *Real Analysis*, 4th ed. (Prentice Hall, Englewood Cliffs, 2010).
[24] G. Nicolis and I. Prigogine, *Self-Organization in Non-Equilibrium Systems: From Dissipative Structures to Order Through Fluctuations* (Wiley, New York, 1977).
[25] P. J. Olver, *Introduction to Partial Differential Equations* (Springer, Heidelberg, 2014).
[26] H. C. Fogedby, Phys. Rev. E **57**, 2331 (1998).
[27] Ł. Kuśmierz, J. M. Rubi, and E. Gudowska-Nowak, J. Stat. Mech. Theor. Exp. (2014) P09002.
[28] S. Kullback and R. A. Leibler, Ann. Math. Stat. **22**, 79 (1951).
[29] A. Nordenfelt, Chaos **25**, 073109 (2015).
[30] E. Ben-Naim, S. Y. Chen, G. D. Doolen, and S. Redner, Phys. Rev. Lett. **83**, 4069 (1999).
[31] V. Burzomato, M. Beato, P. J. Groot-Kormelink, D. Colquhoun, and L. G. Sivilotti, J. Neurosci. **24**, 10924 (2004).
[32] I. Lima Dias Pinto, D. Escaff, U. Harbola, A. Rosas, and K. Lindenberg, Phys. Rev. E **89**, 052143 (2014).
[33] D. Escaff, I. Lima Dias Pinto, and K. Lindenberg, Phys. Rev. E **90**, 052111 (2014).
[34] B. Fernandez and L. S. Tsimring, Phys. Rev. Lett. **100**, 165705 (2008).
[35] T. Prager, B. Naundorf, and L. Schimansky-Geier, Physica A **325**, 176 (2003).
[36] W. Yu and K. B. Wood, Phys. Rev. E **91**, 062708 (2015).
[37] J. A. Acebrón, L. L. Bonilla, C. J. Pérez Vicente, F. Ritort, and Renato Spigler, Rev. Mod. Phys. **77**, 137 (2005).
[38] T. Kiss and K. Nagy, Eur. Biophys. J. **12**, 13 (1985).
[39] E. Yeramian, A. Trautmann, and P. Claverie, Biophys. J. **50**, 253 (1986).
[40] O. S. Ostroumova, V. V. Malev, Y. A. Kaulin, P. A. Gurnev, J. Y. Takemoto, and L. V. Schagina, FEBS Lett. **579**, 5675 (2005).
[41] K. Guseva, M. Thiel, I. Booth, S. Miller, C. Grebogi, and A. de Moura, Phys. Rev. E **83**, 020901 (2011).
[42] K. Manivannan, R. T. Mathias, and E. Gudowska-Nowak, Bull. Math. Biol. **58**, 141 (1996).
[43] M. Sheng and E. Kim, Curr. Opin. Neurobiol. **6**, 602 (1996).
[44] R. Phillips, J. Kondev, and J. Theriot, *Physical Biology of the Cell*, 1st ed. (Garland Science, New York, 2008).
[45] B. Hille, *Ion Channels of Excitable Membranes*, 3rd ed. (Sinauer Associates, Sunderland, 2001).
[46] J. G. Nicholls, A. R. Martin, and B. G. Wallace, *From Neuron to Brain* (Sinauer Associates, Sunderland, 1992).
[47] N. N. Levina, R. R. Lew, and I. B. Heath, J. Cell Sci. **107**, 127 (1994).
[48] M. N. Rasband and J. S. Trimmer, Dev. Biol. **236**, 5 (1996).
[49] M. R. Kaplan, M. H. Cho, E. M. Ullian, L. L. Isom, S. R. Levinson, and B. A. Barres, Neuron **30**, 105 (2001).
[50] D. Bray, M. D. Levin, and C. J. Morton-Firth, Nature (London) **393**, 85 (1998).
[51] J. W. Shuai and P. Jung, Proc. Natl. Acad. Sci. USA **100**, 506 (2002).